

Evidence for Primordial Alignment II: Insights from Stellar Obliquity Measurements for Hot Jupiters in Compact Multiplanet Systems

Brandon T. Radzom¹ , Jiayin Dong^{2,3,6} , Malena Rice⁴ , Xian-Yu Wang¹ , Kyle Hixenbaugh¹ , George Zhou⁵ , Chelsea X. Huang⁵ , and Songhu Wang¹ 

¹ Department of Astronomy, Indiana University, 727 East 3rd Street, Bloomington, IN 47405-7105, USA

² Center for Computational Astrophysics, Flatiron Institute, 162 Fifth Avenue, New York, NY 10010, USA

³ Department of Astronomy, University of Illinois at Urbana-Champaign, Urbana, IL 61801, USA

⁴ Department of Astronomy, Yale University, 219 Prospect Street, New Haven, CT 06511, USA

⁵ University of Southern Queensland, Centre for Astrophysics, West Street, Toowoomba, QLD 4350, Australia

Received 2024 December 5; accepted 2024 December 9; published 2025 March 3

Abstract

A significant fraction of hot Jupiters have orbital axes misaligned with their host stars' spin axes. The large stellar obliquities of these giants have long been considered potential signatures of high-eccentricity migration, which is expected to clear out any nearby planetary companions. This scenario requires that only isolated hot Jupiters be spin-orbit misaligned while those with nearby companions, which must have more quiescent histories, maintain low-obliquity orbits, assuming they formed aligned within their primordial protoplanetary disks. Investigations of this stellar obliquity-companionship connection, however, have been severely limited by the lack of hot Jupiters found in compact multiplanet systems. Here, we present the sky-projected stellar obliquity (λ) of a hot Jupiter with a nearby inner companion recently discovered by NASA's Transiting Exoplanet Survey Satellite: TOI-5143c. Specifically, we utilize the Doppler shadow caused by the planet's transit, enabled by the Rossiter-McLaughlin (RM) effect, to find that the planet is aligned with $\lambda = 2.1^{+2.8}_{-2.7}$ °. Of the exoplanets with RM measurements, TOI-5143c becomes just the third hot Jupiter with a nearby companion, and is part of the 19th compact multiplanet single-star system, with an RM measurement. The spin-orbit alignment of these 19 systems provides strong support for primordial alignment, and thus implies that large obliquities are gained primarily due to postdisk dynamical interactions such as those inherent to high-eccentricity migration. As such, the observed spin-orbit alignment of hot Jupiters with nearby companions affirms that some fraction of these giants instead has quiescent origins.

Unified Astronomy Thesaurus concepts: [Transits \(1711\)](#); [Radial velocity \(1332\)](#); [Exoplanet astronomy \(486\)](#); [Exoplanet evolution \(491\)](#); [Extrasolar gaseous giant planets \(509\)](#); [Exoplanet formation \(492\)](#)

1. Introduction

The origins of hot Jupiters remain one of the most well-studied yet contentious questions in exoplanet science. These short-period ($P < 10$ days) gas giants ($M_p > 0.3 M_J$) have been subject to intense observational campaigns over the past three decades that have enabled substantial population-level characterization (see R. I. Dawson & J. A. Johnson 2018, and references therein). Critically, in contrast with our solar system's Jupiter, a significant fraction of hot Jupiters are observed to have large stellar obliquities—that is, their orbital angular momentum normal axis is often misaligned with the spin axis of their host stars (e.g., G. Hébrard et al. 2008; K. C. Schlaufman 2010; J. N. Winn et al. 2010; S. Albrecht et al. 2012; see reviews by J. N. Winn & D. C. Fabrycky 2015; A. H. M. J. Triaud 2018; S. H. Albrecht et al. 2022), and an even greater majority of hot Jupiters are found to be isolated, devoid of any nearby planetary companions (J. H. Steffen et al. 2012; C. Huang et al. 2016; B. J. Hord et al. 2021; D.-H. Wu et al. 2023).

Together, these observational properties are suggestive of relatively violent dynamical histories for these systems. In this regard, perhaps the most plausible origin is high-eccentricity migration, wherein these giants once occupied wider orbits and acquired large eccentricities following the dispersal of their protoplanetary disks. Mechanisms such as Lidov-Kozai oscillations (Y. Wu & N. Murray 2003; D. Fabrycky & S. Tremaine 2007; S. Naoz 2016), planet–planet scattering (F. A. Rasio & E. B. Ford 1996; S. Chatterjee et al. 2008), or secular chaos (Y. Wu & Y. Lithwick 2011; Y. Lithwick & Y. Wu 2014; A. S. Hamers et al. 2017) may have excited their eccentricities sufficiently to trigger inward migration and subsequently circularization through tidal interactions with their host star, clearing out any nearby planetary companions (A. J. Mustill et al. 2015). While the true prevalence of the various proposed spin-orbit misalignment mechanisms is disputed (S. H. Albrecht et al. 2021; J. Dong & D. Foreman-Mackey 2023; J. C. Siegel et al. 2023), the above processes responsible for high-eccentricity migration may play a major role (see also S. Wang et al. 2021; S. H. Albrecht et al. 2022; M. Rice et al. 2022a).

If this interpretation holds, spin-orbit misalignment for hot Jupiters should be primarily restricted to those that are isolated (i.e., without nearby/close-in planetary companions). Conversely, hot Jupiters that have nearby companions would be expected to maintain orbits in close alignment with the stellar equator, as the presence of these companions inherently

⁶ Flatiron Research Fellow.

 Original content from this work may be used under the terms of the [Creative Commons Attribution 4.0 licence](#). Any further distribution of this work must maintain attribution to the author(s) and the title of the work, journal citation and DOI.

precludes a dynamically violent history. The connection between stellar obliquity and the companionship rate of these giants, however, is poorly understood as the former population of isolated hot Jupiters is observationally abundant, while the latter appears nearly nonexistent—until recently.

The first of such compact multiplanet systems to be confirmed was WASP-47, which contains a $P = 4.2$ day hot Jupiter surrounded by an inner super-Earth at $P = 0.79$ days and an outer hot Neptune at $P = 9.0$ days (C. Hellier et al. 2012; J. C. Becker et al. 2015). Soon after the discovery of this system's compact configuration, R. Sanchis-Ojeda et al. (2015) followed up with radial velocity (RV) observations to measure its stellar obliquity via the Rossiter–McLaughlin (RM) effect (J. R. Holt 1893; D. B. McLaughlin 1924; R. A. Rossiter 1924; D. Queloz et al. 2000), finding the system was spin–orbit aligned. The Kepler space telescope, still responsible for the discovery of most confirmed planets today, found only one hot Jupiter in a compact multiplanet system (Kepler-730; W. Zhu et al. 2018; C. I. Cañas et al. 2019), though the host star remains too faint for ground-based spectroscopic follow-up ($V = 15.8$; M. E. Everett et al. 2012), including detections of the RM effect. Besides WASP-47, the only other compact hot Jupiter systems with RM measurements are WASP-84 (a hot Jupiter and an inner super-Earth; D. R. Anderson et al. 2015; G. Maciejewski et al. 2023) and WASP-148 (a borderline hot Jupiter or hot Saturn with a nearby warm Jupiter companion; G. Hébrard et al. 2020; X.-Y. Wang et al. 2022; E. Knudstrup et al. 2024), both of which were found to be well aligned.

In light of this, the ongoing Transiting Exoplanets Survey Satellite (TESS) mission (G. R. Ricker et al. 2015) has revolutionized the field, uncovering several close-in gas giants with nearby companions (e.g., TOI-2202; T. Trifonov et al. 2021, WASP-148; G. Hébrard et al. 2020, TOI-2000; L. Sha et al. 2023, TOI-5126; T. R. Fairington et al. 2023, TOI-5398; G. Mantovan et al. 2022, 2024a, and HIP 67522; M. G. Barber et al. 2024), including hot Jupiters TOI-1130 (C. X. Huang et al. 2020), WASP-132 (B. J. Hord et al. 2022), TOI-1408 (J. Korth et al. 2024), TOI-2494, and TOI-5143 (S. N. Quinn et al. 2025, in preparation; N. M. Guerrero et al. 2021). Precise stellar obliquity constraints for these systems are possible (e.g., see A. Heitzmann et al. 2021; M. Rice et al. 2023b; G. Mantovan et al. 2024b; B. T. Radzom et al. 2024) thanks to the relative brightness of their host stars and the current suite of extreme precision radial velocity (EPRV) instruments that enable RM measurements on slow rotating stars. Once observed, the RM effect can be modeled in several ways, including the Doppler shadow technique (S. Albrecht et al. 2007; A. Collier Cameron et al. 2010), which relies on distortions in the spectral line profiles during transit, rather than shifts in the radial velocity derived from the observed lines.

In this work, we present a Doppler shadow RM measurement of the sky-projected obliquity (λ) for the compact multiplanet system TOI-5143, using the EPRV NEID spectrograph. TOI-5143 is a KV-type star ($V = 11.9$ mag) that hosts a 5.2 day hot Jupiter (planet c), recently confirmed by S. N. Quinn et al. (2025, in preparation), and a 2.4 day sub-Neptune (planet b). We find $\lambda = 2.1^{+2.8}_{-2.7} \text{ }^\circ$ for TOI-5143c, revealing that the hot Jupiter is spin–orbit aligned. This finding continues the trend of alignment seen for compact multiplanet single-star systems (S. Albrecht et al. 2013; S. Wang et al. 2018; G. Zhou et al. 2018), providing compelling evidence for

primordial alignment and hence postdisk misalignment through high-eccentricity migration channels. Consequently, the growing sample of aligned compact hot Jupiter systems demonstrates that a subset of these giants have dynamically quiescent histories.

This is the 14th published work from the Stellar Obliquities in Long-period Exoplanet Systems (SOLES) survey (M. Rice et al. 2021; M. Rice et al. 2022b; X.-Y. Wang et al. 2022; J. Dong et al. 2023; K. Hixenbaugh et al. 2023; J. Lubin et al. 2023; M. Rice et al. 2023a, 2023b; J. Wright et al. 2023; T. Ferreira dos Santos et al. 2024; Q. Hu et al. 2024; B. T. Radzom et al. 2024; X.-Y. Wang et al. 2024), and is structured as follows. In Section 2, we outline our photometric and spectroscopic observations. In Section 3, we describe our determination of stellar parameters. In Section 4, we detail our modeling of TOI-5143c's Doppler shadow RM signal and, subsequently, its stellar obliquity. In Section 5, we place our findings in context and discuss their implications on the mechanisms driving spin–orbit misalignment as well as the origins of hot Jupiters.

2. Observations

2.1. TESS Photometry

We use the Lightkurve package (Lightkurve Collaboration et al. 2018) to extract TOI-5143c's (TIC ID: 281837575) Presearch Data Conditioning Simple Aperture Photometry (PDCSAP; J. C. Smith et al. 2012; M. C. Stumpe et al. 2012, 2014) light curves from the TESS Science Processing Operations Center (SPOC; J. M. Jenkins et al. 2016), which contains 13 full transits of TOI-5143c spanning Sectors 45 (five transits), 46 (four transits), and 72 (four transits). To process the light-curve data, we perform normalization and clip positive outliers. We then utilize the `transitleastsquares` (M. Hippke & R. Heller 2019) and `wotan` (M. Hippke et al. 2019) packages to identify and remove a partial transit of planet c and all transits of the putative planet b, which is ignored in subsequent modeling.

2.2. Transit Spectroscopy with WIYN/NEID

We obtained in-transit spectroscopy of TOI-5143 using the High Resolution (HR) mode (resolving power of $R \approx 110,000$) on the NEID spectrograph (S. Halverson et al. 2016; C. Schwab et al. 2016) on the 3.5 m WIYN telescope at Kitt Peak National Observatory in Arizona, USA. NEID is a highly stabilized (G. Stefansson et al. 2016; P. Robertson et al. 2019) fiber-fed spectrograph (S. Kanodia et al. 2018; S. Kanodia et al. 2023) with a wavelength coverage of 380–930 nm. On 2022 April 19, we captured 21 RV measurements in HR mode with 480 s exposures spanning 03:46–07:48 UT. These observations occurred under atmospheric conditions with a seeing range of $0.6\text{--}1.5$ (median 0.9) and an airmass range of $z = 1.15\text{--}1.27$. At a wavelength of 5500 Å, the NEID spectrograph achieved a signal-to-noise ratio of 15 pixel $^{-1}$.

The NEID spectra were analyzed using version 1.3.0 of the NEID Data Reduction Pipeline (NEID-DRP).⁷ We extract the Level 2 NEID spectra from the NExSci NEID Archive,⁸ and derive absorption line broadening profiles for all 21 RV

⁷ Detailed information is available at: <https://neid.ipac.caltech.edu/docs/NEID-DRP/>.

⁸ <https://neid.ipac.caltech.edu/>

observations as a function of phase and velocity in order to analyze the Doppler shadow of planet c's transit on the stellar disk. Specifically, we perform least-squares deconvolution (J.-F. Donati et al. 1997) between the NEID spectra and the ATLAS9 synthetic nonrotating spectral template (F. Castelli & R. L. Kurucz 2004) that most closely matches TOI-5143's stellar parameters (see, e.g., G. Zhou et al. 2018; J. Dong et al. 2022).

3. Stellar Properties

To ascertain additional stellar parameters, such as stellar mass and radius, we utilize the MESA Isochrones & Stellar Tracks (MIST) model (J. Choi et al. 2016; A. Dotter 2016), combined with a spectral energy distribution (SED) fitting approach. We compile photometry from various catalogs, including Two Micron All Sky Survey (R. M. Cutri et al. 2003), Wide-field Infrared Survey Explorer (R. M. Cutri et al. 2021), TESS (G. R. Ricker et al. 2015), and Gaia DR2 (Gaia Collaboration et al. 2018). Gaussian priors based on our synthetic spectral fitting were applied to T_{eff} and [Fe/H], along with the parallax from Gaia DR3 (Gaia Collaboration et al. 2023) and an upper limit for the V -band extinction, derived from the 3D dust map by mwdust (J. Bovy et al. 2016). We perform the SED fitting with the differential evolution Markov Chain Monte Carlo (MCMC) technique, integrated within EXOFASTv2 (J. Eastman 2017; J. D. Eastman et al. 2019), from which we obtain uncertainties for fitted parameters. The MCMC procedure was considered converged when the Gelman–Rubin diagnostic (\hat{R} ; A. Gelman & D. B. Rubin 1992) fell below 1.01 and the count of independent draws surpassed 1,000, resulting in the following best-fit parameters for TOI-5143: $M_{\star} = 0.864^{+0.040}_{-0.033} M_{\odot}$, $R_{\star} = 0.852 \pm 0.020 R_{\odot}$, $\rho_{\star} = 1.97^{+0.18}_{-0.16} \text{ g cm}^{-3}$, $\log g^* = 4.514^{+0.029}_{-0.027}$, $T_{\text{eff}} = 5183^{+59}_{-57} \text{ K}$, $[\text{Fe}/\text{H}] = 0.107 \pm 0.044 \text{ dex}$, and Age = $7.4^{+4.4}_{-4.2} \text{ Gyr}$. Based on the results of J. Tayar et al. (2020), we adopt the approximate 2.4% systematic uncertainty floor on our estimate of T_{eff} , which increases its uncertainty to 125 K. Our final stellar parameters are listed in Table 1; note that all are consistent with those reported in S. N. Quinn et al. (2025, in preparation) to within $\pm 2\sigma$.

4. Stellar Obliquity Modeling

We perform a joint fit of the TESS photometry and our NEID RM data for TOI-5143c in order to derive its sky-projected spin-orbit angle λ . As revealed by a preliminary fit of the TESS data only, planet c does not exhibit significant transit timing variations (TTVs), so we directly model its orbital period P and reference mid-transit time T_C in our global RM fit. A more in-depth characterization of TOI-5143c's TTVs is described in Appendix A.

We simultaneously model the planet's transits and Doppler shadow, i.e., the spectral distortion caused by its transit (see Section 2.2), using the Bayesian inference framework implemented within the exoplanet package (D. Foreman-Mackey et al. 2019, 2021), which is powered by PyMC (T. Wiecki et al. 2022). To reduce the computational cost of our Doppler shadow fit, we trim the TESS data to 16 hr segments roughly centered on each of TOI-5143c's 13 full transits (such that each segment spans $\sim 10 \times$ the transit duration), which are constructed based on the linear transit ephemerides from our preliminary transit fit. We apply uniform priors on the P , T_C ,

Table 1
Median Values and 68% HDIs for Relevant and Fitted Parameters of the TOI-5143 (TIC-281837575) System and Its Planet C (TOI-5143c)

Parameters	Description/Units	Values
Stellar Properties		
Gaia Parameters		
α_{J2016}	R.A. (HH:MM:SS.ss)	11:01:27.63
δ_{J2016}	Decl. (DD:MM:SS.ss)	+05:08:22.13
ϖ	Parallax (mas)	5.5942 ± 0.0189
G	G magnitude	11.8203 ± 0.0008
G_{BP}	G_{BP} magnitude	12.2318 ± 0.0034
G_{RP}	G_{RP} magnitude	11.1964 ± 0.0019
Stellar Fit		
M_{\star}	Stellar mass (M_{\odot})	$0.864^{+0.040}_{-0.033}$
R_{\star}	Stellar radius (R_{\odot})	0.852 ± 0.020
ρ_{\star}	Stellar density (g cm^{-3})	$1.97^{+0.18}_{-0.16}$
$\log g$	Stellar surface gravity (cgs)	$4.514^{+0.029}_{-0.027}$
T_{eff}	Stellar effective temperature (K)	5183 ± 125
[Fe/H]	Stellar metallicity (dex)	0.107 ± 0.044
Age	Stellar age (Gyr)	$7.4^{+4.4}_{-4.2}$
Doppler Shadow Fit		
P	Orbital period (days)	$5.2097118^{+0.0000032}_{-0.0000039}$
T_C	Reference mid-transit time	$2527.24264^{+0.00030}_{-0.00027}$
$\rho_{\star, \text{circ}}$	Stellar density (g cm^{-3})	$2.07^{+0.13}_{-0.16}$
b	Impact parameter	0.98 ± 0.03
R_p/R_{\star}	Planet-star radius ratio	$0.175^{+0.025}_{-0.010}$
λ	Projected stellar obliquity ($^{\circ}$)	$2.1^{+2.8}_{-2.7}$
$v \sin i_{\star}$	Projected line broadening (km s^{-1})	$2.53^{+0.28}_{-0.29}$
v_{macro}	Macroturbulent velocity (km s^{-1})	$1.49^{+0.20}_{-0.19}$
Derived Parameters		
a/R_{\star}	Planet-star separation	$14.14^{+0.40}_{-0.37}$
a	Semimajor axis (au)	$0.05602^{+0.00082}_{-0.00079}$
R_p	Planet radius (R_J)	$1.45^{+0.18}_{-0.12}$
i	Orbital inclination ($^{\circ}$)	$86.02^{+0.16}_{-0.15}$
Linear TTV Fit		
P	Orbital period (days)	5.2097117 ± 0.0000036
$T(0)$	Optimal mid-transit time	$2782.51853^{+0.00023}_{-0.00024}$

Note. Gaia parameters are obtained from the Gaia Data Release 3 (Gaia Collaboration et al. 2023) and all other stellar properties are derived in Sections 2.1. and 4. Mid-transit times are reported in units of BJD – 2457000. TTV parameters are derived from an MCMC fit of the 13 observed TESS mid-transit times assuming a linear ephemeris (see Appendix A).

and the mid-transit time of the NEID RM observations T_{RM} . To account for photometric stellar variability, we adopt a Matern 3/2 Gaussian process (GP) kernel (B. Mattn 2013) with variance (GP_s), standard deviation (GP_{σ}), and length-scale (GP_{ρ}) hyperparameters, which we reparameterize to their logarithmic forms and fit for each transit.

To measure TOI-5143c's spin-orbit configuration, we compute a time series of the planet's position $x_p(t)$ on the stellar disk (assuming rigid rotation) and the associated subplanetary velocities:

$$v_p(t) = x_p(t) v \sin i_{\star}, \quad (1)$$

where t is the time of each NEID measurement and $v \sin i_{\star}$ is the projected stellar rotational velocity (i.e., line broadening), which we initialize with uniform priors over $[0.1, 50] \text{ km s}^{-1}$. We then determine the stellar velocity channels being occulted by the planet's shadow, modeling its velocity profile as a

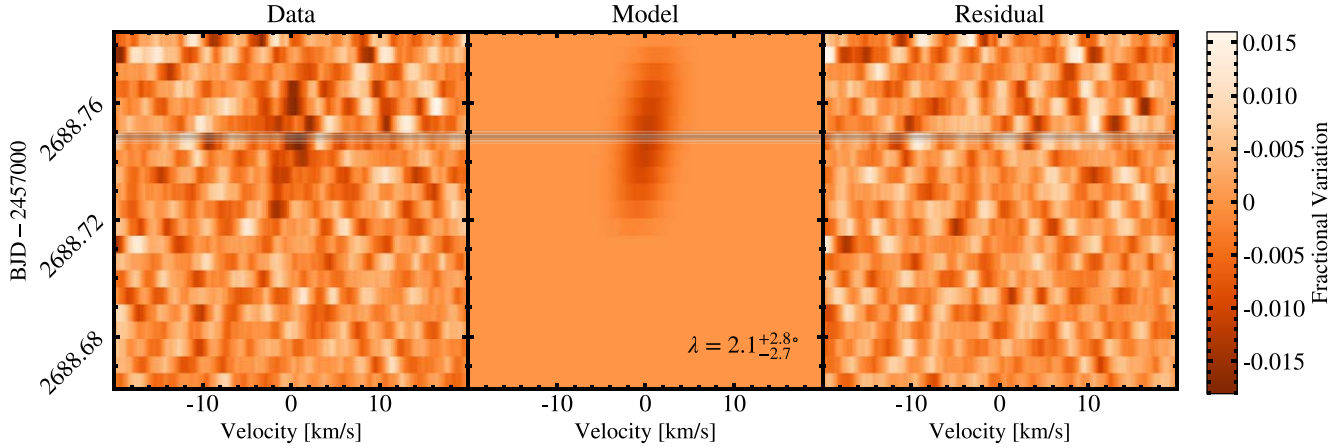


Figure 1. The Doppler shadow of TOI-5143c during its transit, with velocity on the horizontal axes and time on the vertical axis. The left, middle, and right panels correspond to the data extracted from the NEID spectra, our best-fit Doppler shadow model, and the residuals, respectively. The fractional flux variation of the velocity channel is represented on the color axis, and our best-fit transit mid-time is displayed in each panel as the gray dashed line bounded by the 68% (1 σ) and 95% (2 σ) HDI regions.

Gaussian with a width of $\sigma = \sqrt{v_0^2 + v_{\text{macro}}^2}$, where v_0 is a constant determined by NEID's resolution ($R = 110,000$) and v_{macro} is the star's macroturbulent velocity, for which we adopt the same priors as $v \sin i_\star$. We also model the inferred photometric transit light curve, allowing us to scale $v_p(t)$ by the inferred flux time series as well as the ratio of summed velocity profiles from the star and planet. Finally, the Doppler shadow likelihoods are combined to infer the projected stellar obliquity λ , which is initialized at 0° with uniform priors over $[-180, 180]^\circ$.

In addition to P , T_C , T_{RM} , and λ , we allow the following planetary parameters to vary freely in our fit: stellar density assuming a circular orbit $\rho_{*,\text{circ}}$, impact parameter b , and planet-to-star radius ratio R_p/R_\star . Broad uniform priors are adopted for b and R_p/R_\star to accommodate TOI-5143c's grazing configuration (though we impose an upper limit of 0.2 on R_p/R_\star due to the confirmed planetary nature of TOI-5143c), while Gaussian priors based on our SED fitting results (Section 3) are used for $\rho_{*,\text{circ}}$. As is the case for our GP hyperparameters, we reparameterize $v \sin i_\star$, v_{macro} , $\rho_{*,\text{circ}}$, and R_p/R_\star to their logarithmic forms. For both TESS and NEID, we apply a quadratic limb-darkening model with limb-darkening coefficients $\{u_0, u_1\}$ reparameterized as in D. M. Kipping (2013), which are initialized at 0.3 and 0.2, respectively, for both instruments.

We optimize the sampler using the built-in L-BFGS-B algorithm (C. Zhu et al. 1997) and sample the parameter posterior distributions using the gradient-based MCMC No-U-Turn Sampler (M. D. Hoffman & A. Gelman 2011). In particular, we run four MCMC chains with 10,000 tuning iterations, 5000 sample draws, and a target acceptance rate of 0.95. We verify convergence via the \hat{R} statistic, which is ≤ 1.001 for all parameters except b ($\hat{R} = 1.029$; largely due to the TOI-5143c's grazing orbit) for all best-fit values. We discuss the posterior distributions and their covariances in Appendix B.

In Table 1, we report the best-fit results for each parameter as the median value and their uncertainties as the 68% highest density intervals (HDI). Notably, as depicted in Figure 1, we find that TOI-5143c is spin-orbit aligned with a best-fit $\lambda = 2.1^{+2.8}_{-2.7}^\circ$. We additionally verify that all fitted parameters are in good agreement ($\leq 2\sigma$ discrepant) with those reported in S. N. Quinn et al. (2025, in preparation).

5. Discussion

TOI-5143c is the *third* hot Jupiter in a compact, multiplanet, single-star system⁹ to have its stellar obliquity measured (see also WASP-47 b; R. Sanchis-Ojeda et al. 2015, and WASP-84 b; D. R. Anderson et al. 2015), where we define “compact” as having a small period ratio with a neighboring planetary companion: $P_2/P_1 < 6$ (see, e.g., X.-Y. Wang et al. 2022). The low stellar obliquity of TOI-5143c ($\lambda = 2.1^{+2.8}_{-2.7}^\circ$) supports the preliminary pattern of alignment seen for hot Jupiters in compact systems. The alignment of these hot Jupiter systems, in combination with a steadily growing census of hot Jupiters hosting nearby companions (e.g., see also Kepler-730; C. I. Cañas et al. 2019, TOI-1130; C. X. Huang et al. 2020, WASP-132 B. J. Hord et al. 2022, TOI-2000; L. Sha et al. 2023, TOI-1408; J. Korth et al. 2024, and TOI-2494; N. M. Guerrero et al. 2021; S. N. Quinn et al. 2025, in preparation) and updated companion rates from TTV searches (D.-H. Wu et al. 2023), suggest that a nonnegligible fraction of hot Jupiters arrive at their current orbits relatively quiescently, rather than through violent high-eccentricity migration pathways.

More broadly, the aligned spin-orbit angle of TOI-5143c continues the trend of alignment seen across other types of exoplanets in compact systems (e.g., sub-Neptunes; S. Albrecht et al. 2013, and sub-Saturns; B. T. Radzom et al. 2024). In particular, combining the catalogs of E. Knudstrup et al. (2024), S. H. Albrecht et al. (2022), and TEPCat¹⁰ (J. Southworth 2011, accessed on 2024 October 8), we find there are now 19 compact multiplanet single-star systems with robust RM measurements. In brief, we produce this sample by considering all secure and uncontested RM measurements for compact multiplanet systems¹¹ featured in these catalogs, prioritizing values reported in E. Knudstrup et al. (2024), followed by those from S. H. Albrecht et al. (2022), and lastly the “preferred” values from TEPCat. We then utilize the

⁹ There is one known hot Jupiter in a compact multiplanet system embedded within a multistar system: TOI-942A b (C. P. Wirth et al. 2021).

¹⁰ <https://www.astro.keele.ac.uk/jkt/tepcat/obliquity.html>

¹¹ We consider “compact multiplanet systems” to host at least one planet pair with $P_2/P_1 < 6$ if the pair contains a Jovian-mass planet ($\geq 0.3 M_J$), or $P_2/P_1 < 4$ otherwise (e.g., B. T. Radzom et al. 2024). We note that the resultant sample is not strongly sensitive to our choice of period ratio cut.

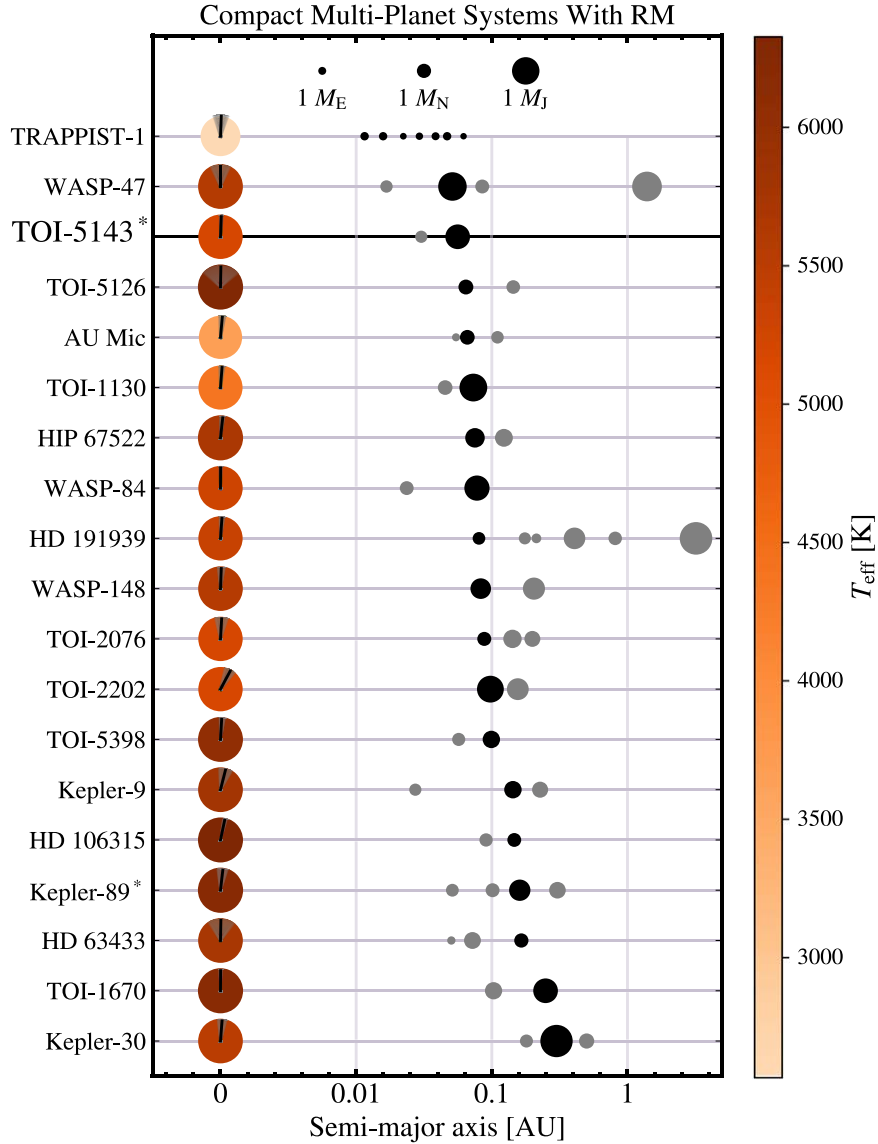


Figure 2. Visual depiction of the configurations and sky-projected spin–orbit angle for all compact multiplanet systems with an RM measurement, laterally stacked by the orbital period of the planet for which the RM effect was measured. A vertical upward spin axis indicates $\lambda = 0^\circ$, and planets with stellar obliquity constraints are shown in black while all others are shown in gray. Stellar effective temperatures are represented by color (see right-hand color axis). Circle sizes scale with the square root of reported planet masses to optimize visual clarity (note that for the unconfirmed planet TOI-5143b, we adopt the J. F. Otegi et al. (2020) mass–radius relation to determine mass), and the corresponding sizes of the Earth, Neptune, and Jupiter are illustrated at the top for reference. Asterisks (*) indicate systems that may plausibly be binaries. Sample selection is described in Section 5.

confirmed planets catalog on the NASA Exoplanet Archive accessed on 2024 October 9, and the multistar catalog of M. Rice et al. (2024; which is based on Gaia DR3 data), to filter out systems with confirmed stellar companions. None of these 19 systems show evidence of misalignment, and *all* are statistically consistent with alignment ($<1\sigma$ deviation from $|\lambda| = 10^\circ$ or $<2\sigma$ deviation from 0°). We display the configurations of these systems in Figure 2.

Additional evidence for primordial alignment follows from current constraints on stellar ages. While few RM measurements exist for young ($\lesssim 100$ Myr old) planetary systems, all of such single-star systems, some still embedded in debris disks, are found to be aligned (e.g., AU Mic; T. Hirano et al. 2020, V1298 Tau; M. C. Johnson et al. 2022, and K2-33; T. Hirano et al. 2024). Further, it has been demonstrated that misaligned hot Jupiter systems tend to be older than those that are aligned (J. H. Hamer & K. C. Schlaufman 2022), and warm Jupiters in single-star

systems, which often host nearby companions (C. Huang et al. 2016; D.-H. Wu et al. 2023), tend to be aligned (M. Rice et al. 2022b; X.-Y. Wang et al. 2024). Therefore, we find that the current census of RM measurements indicates that single-star exoplanetary systems are likely primordially aligned and may become misaligned during the postdisk phase of evolution.

Nearly all known compact multiplanet systems orbiting stars with confirmed or suspected stellar companions are aligned as well (e.g., Kepler-89; T. Hirano et al. 2012, Kepler-25; S. Albrecht et al. 2013, TOI-942; C. P. Wirth et al. 2021; H.-Y. Teng et al. 2024, V1298 Tau; M. C. Johnson et al. 2022, HD 110067; J. Zak et al. 2024, and potentially HD 148193; E. Knudstrup et al. 2024). While unconfirmed, S. N. Quinn et al. (2025, in preparation) found that TOI-5143 may have a bound M-dwarf companion at a projected separation of 116 au, and thus may instead constitute another such aligned compact multiplanet system within a binary. K2-290A, a hot star ($T_{\text{eff}} \approx 6300$ K) in a

triple-star system, represents one major exception, however, hosting two planets (a warm Jupiter and inner sub-Neptune) on compact and retrograde orbits (M. Hjorth et al. 2019, 2021). It is known that the presence of stellar companions introduces additional pathways to excite stellar obliquity (K. Batygin 2012; D. Lai 2014; S. Best & C. Petrovich 2022; S. H. Albrecht et al. 2022), but also that planets orbiting stars hotter than the Kraft break ($T_{\text{eff}} \gtrsim 6250$ K; R. P. Kraft 1967) are more often spin-orbit misaligned than those around cool stars (though this trend appears to apply mostly to hot Jupiters; J. N. Winn et al. 2010; S. Albrecht et al. 2012). Very few RM measurements exist for compact multiplanet systems around hot stars, so it is not yet clear whether the anomalously misaligned configuration of these planets can be attributed to K2-290A's hot temperature or the presence of its stellar companions (or both).

Non-RM measurements of stellar obliquity introduce further ambiguity. For example, D. Huber et al. (2013) employed an asteroseismic technique to determine that the coplanar compact multiplanet system orbiting the formerly hot, now-evolved star Kepler-56, was misaligned ($\lambda \approx 45^\circ$). More recently, E. M. Louden et al. (2024) performed a statistical study on the $v \sin i_*$ of planet-hosting systems, finding that compact multiplanet systems may commonly be spin-orbit misaligned, especially around hot stars. More robust RM measurements of compact multiplanet systems across a wide range of planetary and stellar types, including multistar systems, are needed to fully characterize the prevalence of primordial alignment.

Acknowledgments

Data presented were obtained by the NEID spectrograph built by Penn State University and operated at the WIYN Observatory by NOIRLab, under the NN-EXPLORE partnership of the National Aeronautics and Space Administration and the National Science Foundation. These results are based on observations obtained with NEID on the WIYN 3.5 m Telescope at Kitt Peak National Observatory (PI: Jiayin Dong, NOIRLab 2022A-413894). WIYN is a joint facility of the University of Wisconsin–Madison, Indiana University, NSF's NOIRLab, the Pennsylvania State University, Purdue University, University of California, Irvine, and the University of Missouri. The authors are honored to be permitted to conduct astronomical research on Iolkam Du'ag (Kitt Peak), a mountain with particular significance to the Tohono O'odham.

We acknowledge the use of public TESS data from pipelines at the TESS Science Office and at the TESS Science Processing Operations Center. All TESS data used in this paper can be found at MAST.¹² This research made use of Lightkurve, a Python package for Kepler and TESS data analysis (Lightkurve Collaboration et al. 2018), as well as the NASA Exoplanet Archive (NASA Exoplanet Archive 2024; Composite Planet Data Table¹³), which is operated by the California Institute of Technology, under contract with the National Aeronautics and Space Administration under the Exoplanet Exploration Program.

M.R. acknowledges support from Heising-Simons Foundation grant #2023-4478 and the National Geographic Society. S.W. acknowledges support from Heising-Simons Foundation grant #2023-4050. We acknowledge support from the NASA Exoplanets Research Program NNH23ZDA001N-XRP (grant #80NSSC24K0153). This research was supported in part by

Lilly Endowment, Inc., through its support for the Indiana University Pervasive Technology Institute.

The Flatiron Institute is a division of the Simons Foundation.

Facilities: TESS, WIYN (NEID), Gaia, Exoplanet Archive. **Software:** Arviz (R. Kumar et al. 2019), astropy (Astropy Collaboration et al. 2013, 2018), celerite2 (D. Foreman-Mackey et al. 2017; D. Foreman-Mackey 2018), corner (D. Foreman-Mackey 2016), EXOFASTv2 (J. Eastman 2017; J. D. Eastman et al. 2019), exoplanet (D. Foreman-Mackey et al. 2021, 2019), Jupyter (T. Kluyver et al. 2016), Matplotlib (J. D. Hunter 2007; M. Droettboom et al. 2016), NumPy (S. van der Walt et al. 2011; C. R. Harris et al. 2020), pandas (W. McKinney 2010; pandas development team, T. 2020), PyMC (T. Wiecki et al. 2022), SciPy (P. Virtanen et al. 2020), transitleastsquares (M. Hippke & R. Heller 2019), and wotan (M. Hippke et al. 2019).

Appendix A Transit-only Fit and TTV Analysis

S. N. Quinn et al. (2025, in preparation) did not identify any strong TTVs in their analysis of TOI-5143c, which included TESS Sectors 45 and 46. However, our inclusion of TESS Sector 72 data (acquired ~ 2 yr following Sector 46), as well as our in-transit RM measurement with NEID, enables a substantially longer baseline to be probed. As such, we reanalyze planet c's TTVs using the best-fit orbital period and reference mid-transit time from our global Doppler shadow fit (Section 4). In particular, we perform a separate transit-only fit with the orbital period fixed (to $P = 5.2097118$ days), which allows us to build the Keplerian orbit for planet c and independently model each of its mid-transit times $T_{0..12}$ and hence identify potential TTVs. We otherwise adopt the same set-up with PyMC and exoplanet, fitting for $\rho_{*,\text{circ}}$, b , R_p/R_* , and TESS quadratic limb-darkening coefficients u_0 and u_1 . As was the case for our Doppler shadow fit, all fitted parameters obey $\hat{R} \leq 1.001$ except b , indicating overall convergence. We find $\rho_{*,\text{circ}} = 2.03 \pm 0.14 \text{ g cm}^{-3}$, $b = 0.98 \pm 0.03$, and $R_p/R_* = 0.163 \pm 0.022$, and report our best-fit observed mid-transit times in Table 2. We verify that each parameter is

Table 2
Median Values and 68% HDIs for the Observed TESS Mid-transit Times of TOI-5143c, Obtained from Our Transit-only Fit

Mid-transit Time	Value
T_0	$2527.24122^{+0.00089}_{-0.00092}$
T_1	$2532.45115^{+0.00089}_{-0.00088}$
T_2	$2537.66269^{+0.00087}_{-0.00093}$
T_3	$2542.87331^{+0.00096}_{-0.00092}$
T_4	$2548.08096^{+0.00086}_{-0.00086}$
T_5	$2558.50089^{+0.00081}_{-0.00087}$
T_6	$2563.71231^{+0.00081}_{-0.00076}$
T_7	$2568.92023^{+0.00083}_{-0.00087}$
T_8	$2574.12953^{+0.00081}_{-0.00076}$
T_9	$3267.02198^{+0.00078}_{-0.00079}$
T_{10}	$3272.23155^{+0.00085}_{-0.00084}$
T_{11}	$3277.44167^{+0.00089}_{-0.00079}$
T_{12}	$3282.64982^{+0.00088}_{-0.00082}$

Note. The orbital period was fixed to the best-fit value from our global Doppler shadow fit (see Section 4). All mid-transit times are reported in units of BJD – 2457000.

¹² doi: 10.17909/2kqk-j472.

¹³ doi: 10.26133/NEA2.

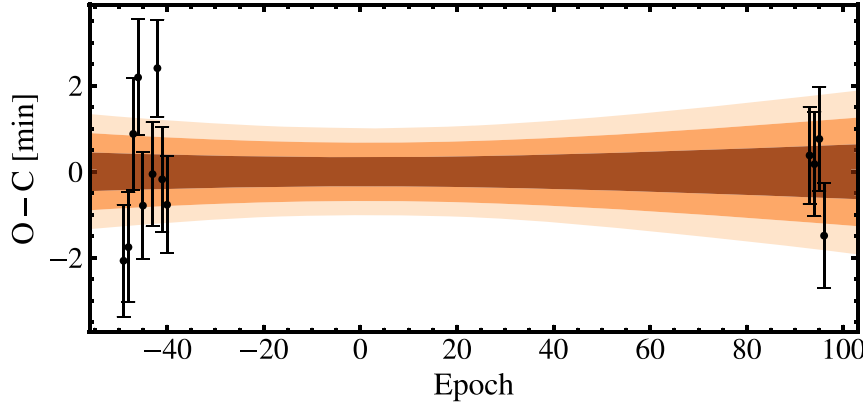


Figure 3. The difference between the observed and calculated mid-transit times assuming a linear ephemeris as a function of transit epoch. Regions containing $\pm 1\sigma$ (68.3%), $\pm 2\sigma$ (95.4%), and $\pm 3\sigma$ (99.7%) confidence intervals are overplotted in red, orange, and beige, respectively. All TTVs show $<2\sigma$ deviation from our predicted linear ephemeris.

consistent (within $\pm 2\sigma$) with the results of both our Doppler shadow fit and S. N. Quinn et al. (2025, in preparation).

To investigate the TTVs of TOI-5143c's orbit, we utilize an MCMC method with the emcee package to fit a linear ephemeris to the 13 observed TESS mid-transit times and compare the observed values to the resultant linear prediction. Specifically, we optimize the equation

$$T(N) = N \times P + T(0), \quad (\text{A1})$$

where $T(0)$ is the optimal zero-epoch mid-transit time, P is the optimal period, N is the transit epoch number, and $T(N)$ is the time at epoch N . This MCMC approach allows us to accurately characterize uncertainties on the expected orbital ephemeris and better identify potential deviations. Note that we select $T(0)$ to be the epoch that minimizes the covariance between $T(0)$ and P (A. Shporer et al. 2009).

We report the resulting orbital period and optimal mid-transit time in Table 1 and display differences between the observed and predicted mid-times in Figure 3. We find no compelling evidence for TTVs—all residuals are consistent with the expected linear ephemeris to within 2σ and the TTVs exhibit no clear sinusoidal signal. This is expected given that the two planets are relatively far from 2:1 period commensurability,

and that TTV amplitude scales with the orbital period and mass of the perturbing planet (M. J. Holman & N. W. Murray 2005; D.-H. Wu et al. 2023), which are both small in the case of TOI-5143c and b, respectively.

Appendix B Parameter Correlations From The Stellar Obliquity Fit

Figure 4 displays a corner plot showing the covariance between the stellar and planetary parameter posteriors that resulted from our joint Doppler shadow model (Section 4). The grazing orbit ($b = 0.98 \pm 0.03$) and unconstrained eccentricity of TOI-5143c lead to a degeneracy between $\rho_{*,\text{circ}}$, b , and R_p/R_* . However, λ and $v \sin i_*$ show no obvious correlation, indicating that our measurement of planet c's spin-orbit angle is robust. Additionally, the strong agreement between our best-fit parameters (especially stellar density) and those of S. N. Quinn et al. (2025, in preparation), in which TOI-5143c's eccentricity was allowed to vary, validate our assumption of a circular orbit for TOI-5143c (note that S. N. Quinn et al. 2025, in preparation compute a low eccentricity of $e = 0.07^{+0.034}_{-0.033}$ in their global fit).

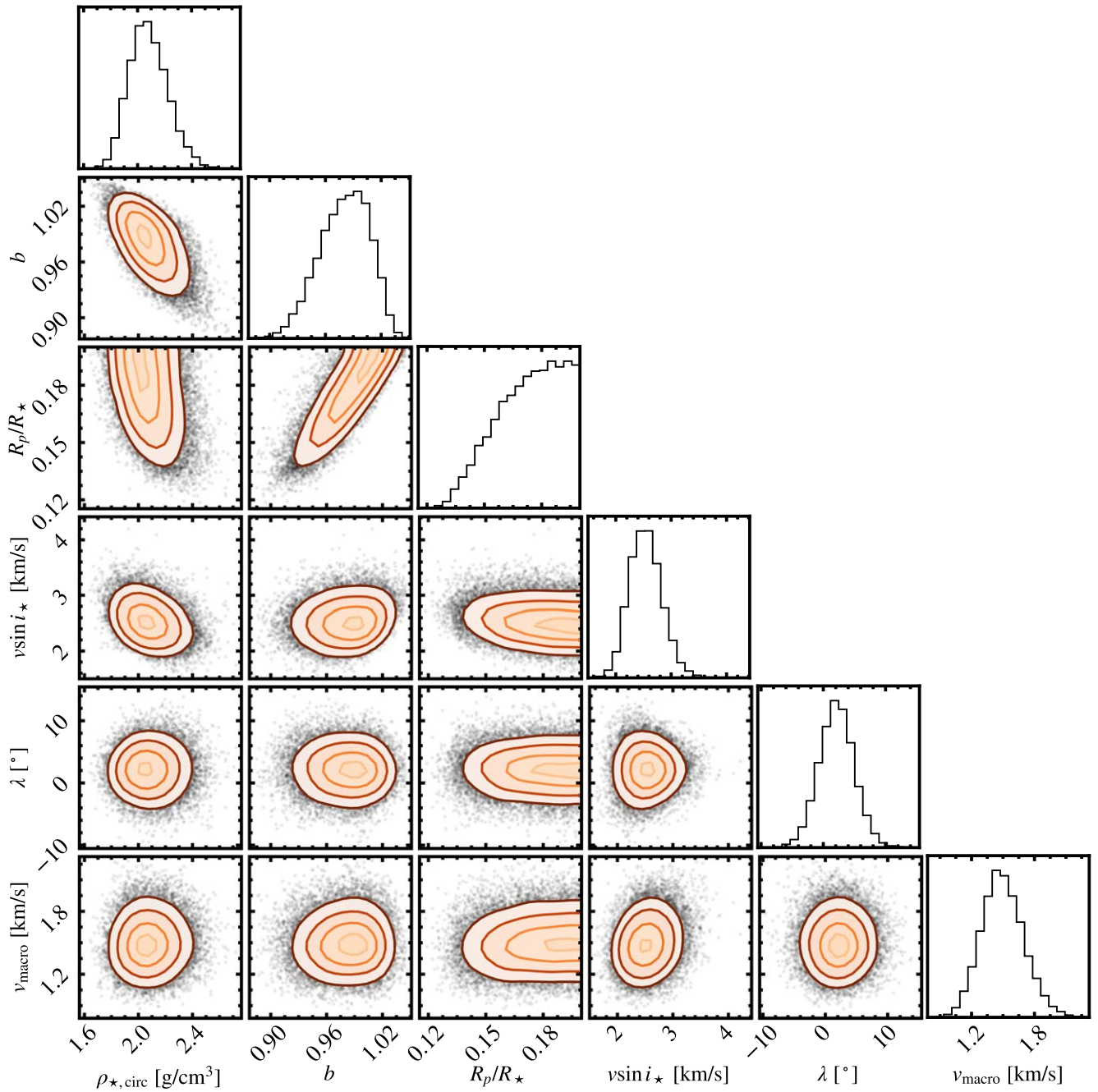


Figure 4. Corner plot of the posteriors from our Doppler shadow modeling. Yellow, orange, red, and maroon contours correspond to the 11.8%, 39.3%, 67.5%, and 86.4% HDIs, respectively.

ORCID iDs

Brandon T. Radzom <https://orcid.org/0000-0002-0015-382X>
 Jiayin Dong <https://orcid.org/0000-0002-3610-6953>
 Malena Rice <https://orcid.org/0000-0002-7670-670X>
 Xian-Yu Wang <https://orcid.org/0000-0002-0376-6365>
 Kyle Hixenbaugh <https://orcid.org/0000-0002-8685-5397>
 George Zhou <https://orcid.org/0000-0002-4891-3517>
 Chelsea X. Huang <https://orcid.org/0000-0003-0918-7484>
 Songhu Wang <https://orcid.org/0000-0002-7846-6981>

References

- Albrecht, S., Reffert, S., Snellen, I., Quirrenbach, A., & Mitchell, D. S. 2007, *A&A*, **474**, 565
 Albrecht, S., Winn, J. N., Marcy, G. W., et al. 2013, *ApJ*, **771**, 11
 Albrecht, S., Winn, J. N., Johnson, J. A., et al. 2012, *ApJ*, **757**, 18
 Albrecht, S. H., Dawson, R. I., & Winn, J. N. 2022, *PASP*, **134**, 082001
 Albrecht, S. H., Marcusen, M. L., Winn, J. N., Dawson, R. I., & Knudstrup, E. 2021, *ApJL*, **916**, L1
 Anderson, D. R., Triaud, A. H. M. J., Turner, O. D., et al. 2015, *ApJL*, **800**, L9
 Astropy Collaboration, Price-Whelan, A. M., Sipőcz, E. J., et al. 2018, *AJ*, **156**, 123
 Astropy Collaboration, Robitaille, T. P., Tollerud, E. J., et al. 2013, *A&A*, **558**, A33
 Barber, M. G., Thao, P. C., Mann, A. W., et al. 2024, *ApJL*, **973**, L30
 Batygin, K. 2012, *Natur*, **491**, 418420
 Becker, J. C., Vanderburg, A., Adams, F. C., Rappaport, S. A., & Schwengeler, H. M. 2015, *ApJL*, **812**, L18
 Best, S., & Petrovich, C. 2022, *ApJL*, **925**, L5
 Bovy, J., Rix, H.-W., Green, G. M., Schlafly, E. F., & Finkbeiner, D. P. 2016, *ApJ*, **818**, 130
 Cañas, C. I., Wang, S., Mahadevan, S., et al. 2019, *ApJL*, **870**, L17

- Castelli, F., & Kurucz, R. L. 2004, *A&A*, **419**, 725
- Chatterjee, S., Ford, E. B., Matsumura, S., & Rasio, F. A. 2008, *ApJ*, **686**, 580
- Choi, J., Dotter, A., Conroy, C., et al. 2016, *ApJ*, **823**, 102
- Collier Cameron, A., Bruce, V. A., Miller, G. R. M., Triaud, A. H. M. J., & Queloz, D. 2010, *MNRAS*, **403**, 151
- Cutri, R. M., Skrutskie, M. F., van Dyk, S., et al. 2003, yCat, II/246
- Cutri, R. M., Wright, E. L., Conrow, T., et al. 2021, yCat, II/328
- Dawson, R. I., & Johnson, J. A. 2018, *ARA&A*, **56**, 175
- Donati, J.-F., Semel, M., Carter, B. D., Rees, D. E., & Cameron, A. C. 1997, *MNRAS*, **291**, 658
- Dong, J., & Foreman-Mackey, D. 2023, *AJ*, **166**, 112
- Dong, J., Huang, C. X., Zhou, G., et al. 2022, *ApJL*, **926**, L7
- Dong, J., Wang, S., Rice, M., et al. 2023, *ApJL*, **951**, L29
- Dotter, A. 2016, *ApJS*, **222**, 8
- Droettboom, M., Hunter, J., Caswell, T. A., et al. 2016 *Matplotlib: Matplotlib v1.5.1*, Zenodo, doi:[10.5281/zenodo.44579](https://doi.org/10.5281/zenodo.44579)
- Eastman, J., 2017 EXOFASTv2: Generalized Publication-quality Exoplanet Modeling Code, Astrophysics Source Code Library, ascl:[1710.003](https://ascl.net/1710.003)
- Eastman, J. D., Rodriguez, J. E., Agol, E., et al. 2019, arXiv:1907.09480
- Everett, M. E., Howell, S. B., & Kinemuchi, K. 2012, *PASP*, **124**, 316
- Fabrycky, D., & Tremaine, S. 2007, *ApJ*, **669**, 1298
- Fairington, T. R., Nabbie, E., Huang, C. X., et al. 2023, *MNRAS*, **527**, 8768
- Ferreira dos Santos, T., Rice, M., Wang, X.-Y., & Wang, S. 2024, *AJ*, **168**, 145
- Foreman-Mackey, D. 2016, *JOSS*, **1**, 24
- Foreman-Mackey, D. 2018, *RNAAS*, **2**, 31
- Foreman-Mackey, D., Agol, E., Ambikasaran, S., & Angus, R. 2017, *AJ*, **154**, 220
- Foreman-Mackey, D., Czekala, I., Luger, R., et al. 2019 *dfm/exoplanet: exoplanet v0.2.1*, Zenodo, doi:[10.5281/zenodo.3462740](https://doi.org/10.5281/zenodo.3462740)
- Foreman-Mackey, D., Luger, R., Agol, E., et al. 2021, *JOSS*, **6**, 3285
- Gaia Collaboration, Brown, A. G. A., Vallenari, A., et al. 2018, *A&A*, **616**, A1
- Gaia Collaboration, Vallenari, A., Brown, A. G. A., et al. 2023, *A&A*, **674**, A1
- Gelman, A., & Rubin, D. B. 1992, *StaSc*, **7**, 457
- Guerrero, N. M., Seager, S., Huang, C. X., et al. 2021, *ApJS*, **254**, 39
- Halverson, S., Terrien, R., Mahadevan, S., et al. 2016, *Proc. SPIE*, **9908**, 99086P
- Hamer, J. H., & Schlaufman, K. C. 2022, *AJ*, **164**, 26
- Hamers, A. S., Antonini, F., Lithwick, Y., Perets, H. B., & Portegies Zwart, S. F. 2017, *MNRAS*, **464**, 688
- Harris, C. R., Millman, J. K., van der Walt, S. J., et al. 2020, *Natur*, **585**, 7825
- Hébrard, G., Bouchy, F., Pont, F., et al. 2008, *A&A*, **488**, 763
- Hébrard, G., Diaz, R. F., Correia, A. C. M., et al. 2020, *A&A*, **640**, A32
- Heitzmann, A., Zhou, G., Quinn, S. N., et al. 2021, *ApJL*, **922**, L1
- Hellier, C., Anderson, D. R., Collier Cameron, A., et al. 2012, *MNRAS*, **426**, 739
- Hippke, M., David, T. J., Mulders, G. D., & Heller, R. 2019, *AJ*, **158**, 143
- Hippke, M., & Heller, R. 2019, *A&A*, **623**, A39
- Hirano, T., Gaidos, E., Harakawa, H., et al. 2024, *MNRAS*, **530**, 3117
- Hirano, T., Krishnamurthy, V., Gaidos, E., et al. 2020, *ApJL*, **899**, L13
- Hirano, T., Narita, N., Sato, B., et al. 2012, *ApJL*, **759**, L36
- Hixenbaugh, K., Wang, X.-Y., Rice, M., & Wang, S. 2023, *ApJL*, **949**, L35
- Hjorth, M., Albrecht, S., Hirano, T., et al. 2021, *PNAS*, **118**, e2017418118
- Hjorth, M., Justesen, A. B., Hirano, T., et al. 2019, *MNRAS*, **484**, 3522
- Hoffman, M. D., & Gelman, A. 2011, arXiv:1111.4246
- Holman, M. J., & Murray, N. W. 2005, *Sci*, **307**, 1288
- Holt, J. R. 1893, *AstAp*, **12**, 646
- Hord, B. J., Colón, K. D., Berger, T. A., et al. 2022, *AJ*, **164**, 13
- Hord, B. J., Colón, K. D., Kostov, V., et al. 2021, *AJ*, **162**, 263
- Hu, Q., Rice, M., Wang, X.-Y., et al. 2024, *AJ*, **167**, 175
- Huang, C., Wu, Y., & Triaud, A. H. M. J. 2016, *ApJ*, **825**, 98
- Huang, C. X., Quinn, S. N., Vanderburg, A., et al. 2020, *ApJL*, **892**, L7
- Huber, D., Carter, J. A., Barbieri, M., et al. 2013, *Sci*, **342**, 331
- Hunter, J. D. 2007, *CSE*, **9**, 90
- Jenkins, J. M., Twicken, J. D., McCauliff, S., et al. 2016, *Proc. SPIE*, **9913**, 99133E
- Johnson, M. C., David, T. J., Petigura, E. A., et al. 2022, *AJ*, **163**, 247
- Kanodia, S., Mahadevan, S., Ramsey, L. W., et al. 2018, *Proc. SPIE*, **10702**, 107026Q
- Kanodia, S., Lin, A. S. J., Lubars, E., et al. 2023, *AJ*, **166**, 105
- Kipping, D. M. 2013, *MNRAS*, **435**, 2152
- Kluyver, T., Ragan-Kelley, B., & Pérez, F. 2016, in Positioning and Power in Academic Publishing: Players, Agents and Agendas, ed. F. Loizides & B. Schmidt (Amsterdam: IOS Press), 87
- Knudstrup, E., Albrecht, S. H., Winn, J. N., et al. 2024, *A&A*, **690**, A379
- Korth, J., Chaturvedi, P., Parviainen, H., et al. 2024, *ApJL*, **971**, L28
- Kraft, R. P. 1967, *ApJ*, **150**, 551
- Kumar, R., Carroll, C., Hartikainen, A., & Martin, O. 2019, *JOSS*, **4**, 1143
- Lai, D. 2014, *MNRAS*, **440**, 3532
- Lightkurve Collaboration, Cardoso, J. V. d. M., Hedges, C., et al., 2018 Lightkurve: Kepler and TESS Time Series Analysis in Python, *Astrophysics Source Code Library*, ascl:[1812.013](https://ascl.net/1812.013)
- Lithwick, Y., & Wu, Y. 2014, *PNAS*, **111**, 12610
- Louden, E. M., Wang, S., Winn, J. N., et al. 2024, *ApJL*, **968**, L2
- Lubin, J., Wang, X.-Y., Rice, M., et al. 2023, *ApJL*, **959**, L5
- Maciejewski, G., Golonka, J., Łoboda, W., et al. 2023, *MNRAS*, **525**, L43
- Mantovan, G., Malavolta, L., Desidera, S., et al. 2024a, *A&A*, **682**, A129
- Mantovan, G., Malavolta, L., Locci, D., et al. 2024b, *A&A*, **684**, L17
- Mantovan, G., Montalito, M., Piotto, G., et al. 2022, *MNRAS*, **516**, 4432
- Matrn, B. 2013, Spatial Variation (2nd ed.; Berlin: Springer)
- McKinney, W. 2010, in Proc. 9th Python in Science Conf., ed. S. van der Walt & J. Millman (Austin, TX: SciPy), 56
- McLaughlin, D. B. 1924, *ApJ*, **60**, 22
- Mustill, A. J., Davies, M. B., & Johansen, A. 2015, *ApJ*, **808**, 14
- Naoz, S. 2016, *ARA&A*, **54**, 441
- NASA Exoplanet Archive 2024, *Planetary Systems Composite Parameters, Version: 2024-03-12*, NExSci-Caltech/IPAC, doi:[10.26133/NEA13](https://doi.org/10.26133/NEA13)
- Otegi, J. F., Bouchy, F., & Helled, R. 2020, *A&A*, **634**, A43
- pandas development team, T., 2024 *pandas-dev/pandas: Pandas*, v2.2.2, Zenodo, doi:[10.5281/zenodo.1095763](https://doi.org/10.5281/zenodo.1095763)
- Queloz, D., Eggenberger, A., Mayor, M., et al. 2000, *A&A*, **359**, L13
- Radzom, B. T., Dong, J., Rice, M., et al. 2024, *AJ*, **168**, 116
- Rasio, F. A., & Ford, E. B. 1996, *Sci*, **274**, 954
- Rice, M., Gerbig, K., & Vanderburg, A. 2024, *AJ*, **167**, 126
- Rice, M., Wang, S., Gerbig, K., et al. 2023a, *AJ*, **165**, 65
- Rice, M., Wang, S., & Laughlin, G. 2022a, *ApJL*, **926**, L17
- Rice, M., Wang, S., Howard, A. W., et al. 2021, *AJ*, **162**, 182
- Rice, M., Wang, S., Wang, X.-Y., et al. 2022b, *AJ*, **164**, 104
- Rice, M., Wang, X.-Y., Wang, S., et al. 2023b, *AJ*, **166**, 266
- Ricker, G. R., Winn, J. N., Vanderspek, R., et al. 2015, *JATIS*, **1**, 014003
- Robertson, P., Anderson, T., Stefansson, G., et al. 2019, *JATIS*, **5**, 015003
- Rossiter, R. A. 1924, *ApJ*, **60**, 15
- Sanchis-Ojeda, R., Winn, J. N., Dai, F., et al. 2015, *ApJL*, **812**, L11
- Schlaufman, K. C. 2010, *ApJ*, **719**, 602
- Schwab, C., Rakich, A., & Gong, Q. 2016, *Proc. SPIE*, **9908**, 99087H
- Sha, L., Vanderburg, A. M., Huang, C. X., et al. 2023, *MNRAS*, **524**, 1113
- Shporer, A., Mazeh, T., Pont, F., et al. 2009, *ApJ*, **694**, 1559
- Siegel, J. C., Winn, J. N., & Albrecht, S. H. 2023, *ApJL*, **950**, L2
- Smith, J. C., Stumpe, M. C., Van Cleve, J. E., et al. 2012, *PASP*, **124**, 1000
- Southworth, J. 2011, *MNRAS*, **417**, 2166
- Stefansson, G., Hearty, F., Robertson, P., et al. 2016, *ApJ*, **833**, 175
- Steffen, J. H., Ragozzine, D., Fabrycky, D. C., et al. 2012, *PNAS*, **109**, 7982
- Stumpe, M. C., Smith, J. C., Catanzarite, J. H., et al. 2014, *PASP*, **126**, 100
- Stumpe, M. C., Smith, J. C., Van Cleve, J. E., et al. 2012, *PASP*, **124**, 985
- Tayar, J., Claytor, Z. R., Huber, D., & van Saders, J. 2022, *ApJ*, **927**, 31
- Teng, H.-Y., Dai, F., Howard, A. W., et al. 2024, *AJ*, **168**, 194
- Triaud, A. H. M. J. 2018, in Handbook of Exoplanets, ed. H. J. Deeg & J. A. Belmonte, Vol. 2 (Cham: Springer)
- Trifonov, T., Brahm, R., Espinoza, N., et al. 2021, *AJ*, **162**, 283
- van der Walt, S., Colbert, S. C., & Varoquaux, G. 2011, *CSE*, **13**, 22
- Virtanen, P., Gommers, R., Oliphant, T. E., et al. 2020, *NatMe*, **17**, 261
- Wang, S., Addison, B., Fischer, D. A., et al. 2018, *AJ*, **155**, 70
- Wang, S., Winn, J. N., Addison, B. C., et al. 2021, *AJ*, **162**, 50
- Wang, X.-Y., Rice, M., Wang, S., et al. 2022, *ApJL*, **926**, L8
- Wang, X.-Y., Rice, M., Wang, S., et al. 2024, *ApJL*, **973**, L21
- Wiecki, T., Salvatier, J., Patil, A., et al., 2022 *pymc-devs/pymc:*, v4.1.7, Zenodo, doi:[10.5281/zenodo.7467113](https://doi.org/10.5281/zenodo.7467113)
- Winn, J. N., Fabrycky, D. C., Albrecht, S., & Johnson, J. A. 2010, *ApJL*, **718**, L145
- Winn, J. N., & Fabrycky, D. C. 2015, *ARA&A*, **53**, 409
- Wirth, C. P., Zhou, G., Quinn, S. N., et al. 2021, *ApJL*, **917**, L34
- Wright, J., Rice, M., Wang, X.-Y., Hixenbaugh, K., & Wang, S. 2023, *AJ*, **166**, 217
- Wu, D.-H., Rice, M., & Wang, S. 2023, *AJ*, **165**, 171
- Wu, Y., & Lithwick, Y. 2011, *ApJ*, **735**, 109
- Wu, Y., & Murray, N. 2003, *ApJ*, **589**, 605
- Zak, J., Boffin, H. M. J., Sedaghati, E., et al. 2024, *A&A*, **687**, L2
- Zhou, G., Rodriguez, J. E., Vanderburg, A., et al. 2018, *AJ*, **156**, 93
- Zhu, C., Byrd, R. H., Lu, P., & Nocedal, J. 1997, *ACM Trans. Math. Softw.*, **23**, 550560
- Zhu, W., Dai, F., & Masuda, K. 2018, *RNAAS*, **2**, 160